BIOCHEMISTRY
including biophysical chemistry & molecular biology

Article

pubs.acs.org/biochemistry

Effect of 10.5 M Aqueous Urea on *Helicobacter pylori* Urease: A Molecular Dynamics Study

Mona S. Minkara,[†,‡] Michael N. Weaver,[†,‡] and Kenneth M. Merz, Jr.*[,†,‡]

[†]Department of Chemistry, Quantum Theory Project, University of Florida, 2328 New Physics Building, Gainesville, Florida 32611-8435, United States

[‡]Department of Chemistry and Department of Biochemistry and Molecular Biology, Michigan State University, 578 South Shaw Lane, East Lansing, Michigan 48824-1322, United States

Supporting Information

ABSTRACT: The effects of a 10.5 M solution of aqueous urea on *Helicobacter pylori* urease were investigated over the course of a 500 ns molecular dynamics (MD) simulation. The enzyme was solvated by 25321 water molecules, and additionally, 4788 urea molecules were added to the solution. Although concentrated urea solutions are known laboratory denaturants, the protein secondary structure is retained throughout the simulation largely because of the short simulation time (urea denaturation occurs on the millisecond time scale). The relatively constant solvent accessible surface area over the last 400 ns of the simulation further confirms the overall lack of denaturation. The wide-open flap state observed previously in *Klebsiella areogenes* urease [Roberts, B. P., et al. (2012) *J. Am. Chem. Soc. 134*, 9934] and *H. pylori* [Minkara, M. S., et al. (2014) *J. Chem. Theory Comput. 10*, 1852−1862] was also identified in this aqueous urea simulation. Over the course of the trajectory, we were able to observe urea molecules entering the active site in proportions related to the extent of opening of the active site-covering flap. Furthermore, urea molecules were observed to approach the pentacoordinate Ni^{2+} ion in position to bind in a manner consistent with the proposed initial coordination step of the hydrolysis mechanism. We also observed a specific and unique pattern in the regions of the protein with a high root-mean-square fluctuation (rmsf). The high-rmsf regions in the β-chain form a horseshoelike arrangement surrounding the active site-covering flap on the surface of the protein. We hypothesize that the function of these regions is to both attract and shuttle urea toward the loop of the active site-covering flap before entry into the cavity. Indeed, urea is observed to interact with these regions for extended periods of simulation time before active site ingress.

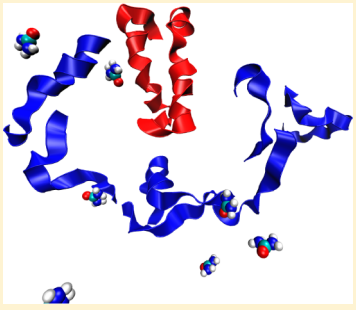

Helicobacter pylori (HP) infects the human stomach by embedding within the gastric mucosa.[1] The bacteria survive the highly acidic stomach environment by producing copious amounts of urease (EC 3.5.1.5), an enzyme that hydrolyzes urea to initially produce ammonia and carbamate and eventually causes a net increase in the pH of the immediate environment. Urease is a highly efficient enzyme, with a Michaelis constant, K_m, of 0.17 mM, and provides a 10^{14}-fold increase in the rate of urea hydrolysis.[1,2] Because of its dodecameric structure, urease is relatively large, with a molecular mass of 1.06 MDa.[3] More than two-thirds of the world's population is infected with HP bacteria, and although in most cases it is not deadly, in some instances it can lead to liver failure and stomach cancer. Additionally, the bacterium has also been shown to be a factor in gastric and peptic ulcers and additional gastrointestinal disorders.[4−7] This is most prevalent in developing countries and is due primarily to the mode of transmission, through contaminated water or food that picks up the bacteria from animal excretions.

Currently, the most common method of eradicating HP bacterial infection is dual antibiotic treatment in combination with a proton pump inhibitor.[8] Antibiotics are increasingly ineffective in eradicating HP infections because of the emergence of antibiotic resistant strains of the bacteria and the ineffectiveness of some antibiotics under low-pH conditions. Recently, a quadruple therapy[9] incorporating bismuth subcitrate has been utilized to combat clarithromycin resistant *H. pylori* strains.

Many theoretical studies have been conducted to identify suitable inhibitors for HP urease and further elucidate the structure and function of the enzyme, using quantum mechanical (QM), molecular dynamics (MD), and docking methodologies. In addition to QM and MD studies of the hydrolysis of urea and the activity of the enzyme out of our group,[10−14] there have been numerous other studies. Abid et al. screened 6000 potential urease inhibitors using MOE-Dock and GOLD and identified new directions for studying structure−activity relationships in these inhibitors.[15] Valdez and Alexandrova used QM/DMD methods to study the role of Ni ions in the enzyme.[16] Font and co-workers identified structural requirements for urease activity in phosphoramide derivatives using molecular orbital-based arguments[17] and used

Received: January 27, 2015
Revised: June 1, 2015
Published: June 9, 2015

DOI: 10.1021/acs.biochem.5b00078
Biochemistry 2015, 54, 4121−4130

experimental IC_{50} values[18] as a basis for comparison. Xiao and co-workers employed a variety of computational and experimental techniques to evaluate the efficacy of quercetin and its analogues as potential urease inhibitors.[19]

Urea is widely known and used as a denaturing agent.[20,21] Generally, the requirements for protein denaturation by urea are concentrations exceeding 8 M and temperatures exceeding 20 °C. For example, Muthuselvi et al. reported that urea concentrations of >10 M were required to denature myoglobin.[22] To elucidate the interaction between urea and proteins, numerous MD simulations have been conducted. Independent studies published by Tirado-Rives and Jorgenson[23] as well as Caflisch and Karplus[24] used MD methods to probe the impact of urea as a denaturant on barnase. Both groups reported that observation of denaturing effects on barnase requires a long MD simulation time and an elevated temperature. A recent study by Camilloni et al. reported that urea denatured protein L in MD simulations with temperatures of 400 and 480 K.[25] They also ran a 300 K simulation in which the relatively small protein remained in the native conformation after 20 ns. Cai et al. used MD methods to probe the effect of urea concentration on protein aggregation.[26] Finally, Moeser and Horinek presented a model for urea denaturation proposing equal side chain and backbone contributions.[27] Other studies have focused on the effect urea has on water structure, another example of its rich hydrogen bonding.[28,29]

Recently, we reported the first full MD simulation on HPU,[30] which entailed a 400 ns simulation that revealed a wide-open flap state similar to that observed in an earlier simulation[31] on *Klebsiella aerogenes* urease. Herein, we describe the results of a 500 ns MD simulation on *H. pylori* urease in 10.5 M aqueous urea. This large simulation took seven months to acquire and represents a significant use of computational resources. From a statistical mechanics perspective, while this simulation does not assemble the full partition function for the association of urea with urease (indeed, one could argue no MD simulation for a complex biochemical problem that achieves this lofty goal exists in the literature), with 12 active sites we are able to analyze an effective 6 μs of dynamics during which a urea can explore an active site. To the best of our knowledge, this is the first MD study incorporating high concentrations of urea in a simulation on urease. The high concentration of urea was chosen to sample the widest possible range of urea−urease interactions without requiring unattainable simulation time scales. This artificially high concentration allowed us to effectively enhance the sampling of urea in the active site. We compare these results to a 500 ns trajectory on *H. pylori* urease in aqueous solution (100 ns beyond what was previously reported).[30]

METHODS

Structure Preparation. As in our previous MD efforts aimed at aqueous HP urease, we selected Protein Data Bank (PDB) structure 1E9Z[7] as the starting point and utilized PyMOL[32] to perform the reflections required to generate the dodecamer. The H++ online protonation server was used to obtain the correct protonation states of the amino acids throughout the structure at pH 7.5[33−36] following our previous procedure.[30] The bonded model was created with the MCPB component of the tLeap facility (AmberTools version 1.5)[37] to define the Ni^{2+} coordination site, and subsequently, the hydrogen atoms and water molecules were added. Neutralization was achieved via the addition of 44 Na^+ ions and the structure solvated by a periodically replicated TIP3P[38] octahedral water box using tLeap. A total of 25321 water molecules were used to hydrate the structure, and 4788 urea molecules were added to the system. The metal parameters developed for *K. aerogenes* urease by Roberts et al.[39] with the MTK++/MCPB utility of AmberTools and to be consistent with our previous effort[30] were modified utilizing previously developed Lennard-Jones parameters[40] (R^* and ε) for Zn^{2+} as parameters for the Ni^{2+} ion.

Minimization and Equilibration. The energy minimization of the structure was performed using the FF99SB[41,42] force field using a two-stage procedure. We first minimized the nickel coordination sites by imposing weak harmonic positional restraints of 10 kcal mol^{-1} $Å^{-2}$ on all atoms outside the Ni coordination sphere. The steepest descent method was first used for 1×10^5 steps to minimize the active site. Subsequently, the entire structure was relaxed and minimized using steepest descent for 1×10^4 steps. The initial step length was decreased to 1×10^{-6} Å. After minimization, the structure was equilibrated in another two-stage process. In the first stage, the temperature was increased from 0 to 300 K over 1×10^6 steps of MD with a step size of 0.002 ps (2 fs) in the canonical (*NVT*) ensemble, placing a weak harmonic positional restraint on the whole protein. After the system was heated to 300 K, the simulation was run for 10 ps in the isobaric, isothermal (*NPT*) ensemble after removal of all the harmonic restraints. Temperature control was achieved using Langevin dynamics with a collision frequency, γ, of 2.0 ps^{-1} during the first and 1.0 ps^{-1} during the second equilibration stage. SHAKE[43] was used to constrain all hydrogen-containing bonds during both equilibration steps. Long-range electrostatic interactions were computed using the particle mesh Ewald method with an 8 Å cutoff.

Molecular Dynamics. A 500 ns MD simulation was run on *H. pylori* urease in 10.5 M aqueous urea using the PMEMD version of Amber 12[44,45] on an M2090 GPU using the FF99SB force field. The production MD run was procured over 500 ns in the isobaric, isothermal (*NPT*) ensemble, which was acquired using 2.0×10^8 steps, with a 0.002 ps time step. The temperature was kept constant at 300 K using Langevin dynamics with a collision frequency of 1.0 ps^{-1}, while the pressure was maintained at 1 bar with a pressure relaxation time of 2.0 ps. SHAKE was again used to constrain all hydrogen-containing bonds. For the calculation of the nonbonded interactions, again we made use of the particle mesh Ewald method and a cutoff distance of 8 Å was employed while computing the long-range electrostatic interactions. Frames were saved every 5×10^3 steps (10 ps), providing 5×10^4 frames.

Analysis. All frames were analyzed for the flap state defining residue separations, root-mean-square deviation (rmsd), atomic root-mean-square fluctuations (rmsf), and correlation matrices using the PTRAJ utility of AmberTools version 1.5. The rmsd was obtained for each atom in the entire protein with the first frame of the trajectory as the reference and gives an average deviation of the protein geometry from the reference structure at each point over the simulation time. We also separated out the residues involved in the motion of the active site-covering flaps and obtained the rmsd for each of these. The rmsf was computed on a per residue basis, using the α-carbon of each residue as the reference point and providing a time-averaged value. The solvent accessible surface area was determined using NAccess version 2.1.1[46] that implements the method of Lee and Richards[47] for the determination of area. The secondary

DOI: 10.1021/acs.biochem.5b00078
Biochemistry 2015, 54, 4121−4130

structure assignments were made utilizing the DSSP program of Kabsch and Sander.[48,49] Urea residence times with regions of high rmsf were determined using a code developed to record all urea molecules within 2 Å of any residue of each region of interest based on 501 PDB files (for the equilibrated structure and taken at each nanosecond). We generated histograms for each region and each dimer that show the number of urea molecules that are within 2 Å for >10 ns. We also plotted for each region of each dimer the total number of urea molecules that reside within 2 Å as a function of time. The chosen distance cutoff is tight to account for the great amount of difficulty in determining optimal hydrogen bonding angles for 4788 urea molecules over 500 PDB files.

Throughout our discussion of the residues, we will identify them both by the residue numbering of Ha et al. (α and β chains)[7] and by the residue numbering from the PDB (1−807). For the purposes of this analysis, the flap covering the active site was considered to span residues α304−347 (542−585) with the first α-helix composed of residues α304−322 (542−560), the turn composed of residues α323−329 (561−567), and the second α-helix composed of residues α330−347 (568−585). The α-helices are extended from the helical section described by Ha et al. to account for all residues in the flap region that adopt α-helical character at some point during the simulation.

RESULTS

Over the course of the molecular dynamics simulation of HPU in an aqueous 10.5 M urea solution, the rmsd slowly climbs from 2.0 to 2.5 Å over the first 400 ns and remains at nearly 2.5 Å for the remainder of the simulation. In the active site-covering flaps of dimers 3−5 and 7, the rmsd spikes in the last 100−200 ns. The average radius of gyration levels off at ∼300 ns into the simulation and remains at a value between 60.2 and 60.4 Å. The maximal radius, approximately 90 Å, is observed on multiple occasions, at approximately 300, 450, and 500 ns. Over the latter half of the simulation, a radius maximum between 87 and 89 Å is generally maintained.

Protein Denaturation? The solvent accessible surface area (SASA) of both HPU in water and in aqueous 10.5 M urea was determined for the equilibrated structures and at each 100th nanosecond of the simulation. We did this to determine if the protein was denaturing during our simulation time scale. It has been shown if the protein undergoes denaturation, it experiences an increase in the surface area that is accessible to the solvent.[23,24] In both simulations, there was a significant increase in the total SASA (Table 1) from the initial stages of the simulation to the 100 ns point. This could be in part due to the protein relaxing from initially being in a crystal conformation. After 100 ns, the increase levels off and there is only a modest increase in the SASA over the remainder of the MD simulation. Furthermore, upon comparison of the simulation incorporating urea to the one featuring only water, the increase is larger in the aqueous simulation, indicating the protein is not denaturing (at the time scales employed) because of the 10.5 M concentration of urea found in the solvent. Beyond this analysis, it seems likely that urease is less sensitive to urea than other proteins simply because urea is a substrate of this protein and as such urea would locally be expected to be present at concentrations higher than the background.

Over the duration of the simulation of the SASA, we find that side chains are much more exposed than the backbone of the enzyme as expected (Table 2). A general increase in exposed surface and thereby the percent increase in exposed side chain and main chain occur over the simulation, with the respective contributions of the side and main chain atoms to the total remaining relatively unchanged. The relative contributions to the total SASA following equilibration show that the side chain comprised 87.2% of the exposed enzyme surface and the main chain contribution was 12.8%. Following equilibration, the side chain SASA comprised 85.1% of the total, with the remaining 14.9% being ascribed to main chain atoms. At the 100 ns mark, the percentages decline to 84.9 and 15.1% for the side chain and main chain, respectively, and remain stable at these percentages over the duration of the 500 ns simulation, where the percentages of exposed side chain and main chain surface area are 84.5 and 15.5%, respectively.

These results show that more nonpolar atoms than polar are exposed on the surface: 39.4% of the exposed surface is comprised of polar atoms, while 60.6% come from nonpolar atoms as evaluated via the X-ray structure (Table 3). After

Table 1. Total Solvent Accessible Surface Areas for the X-ray Structure of *H. pylori* Urease and Evaluated at Points along the MD Simulations on the Aqueous Urease and the Urease in Aqueous 10.5 M Urea

	H. pylori urease		*H. pylori* urease with urea	
	total SASA (Å^2)	% increase[a]	total SASA (Å^2)	% increase
X-ray	234281.9	–	234281.9	–
equilibrated	248967.6	6.3	243999.1	4.1
100 ns	281311.5	20.1	273445.3	16.7
200 ns	287003.8	22.5	281490.2	20.2
300 ns	287774.2	22.8	284452.5	21.4
400 ns	291730.1	24.5	287777.2	22.8
500 ns	292556.0	24.9	288403.3	23.1

[a]Percent increase in SASA referenced to the X-ray structure.

Table 2. Side Chain and Main Chain Accessible Surface Areas for *H. pylori* Urease in 10.5 M Urea

	side chain		main chain	
	SASA (Å^2)	% increase[a]	SASA (Å^2)	% increase
X-ray	204176.9	–	30105.2	–
equilibrated	207698.3	1.7	36300.7	20.6
100 ns	232283.8	13.8	41162.0	36.7
200 ns	238586.8	16.9	42903.6	42.5
300 ns	240693.0	17.9	43760.3	45.4
400 ns	243522.6	19.3	44255.4	47.0
500 ns	243832.3	19.4	44570.5	48.0

[a]Percent increase in SASA referenced to the X-ray structure.

Table 3. Polar and Nonpolar Accessible Surface Areas for *H. pylori* Urease in 10.5 M Urea

	nonpolar		all polar	
	SASA (Å^2)	% increase[a]	SASA (Å^2)	% increase
X-ray	141933.6	–	92348.2	–
equilibrated	141806.6	−0.1	102192.4	10.7
100 ns	156404.5	10.2	117040.7	26.7
200 ns	161719.3	13.9	119771.5	29.7
300 ns	163253.5	15.0	121200.0	31.2
400 ns	165316.7	16.5	122460.5	32.6
500 ns	165990.5	16.9	122411.8	32.6

[a]Percent increase in SASA referenced to the X-ray structure.

DOI: 10.1021/acs.biochem.5b00078
Biochemistry 2015, 54, 4121−4130

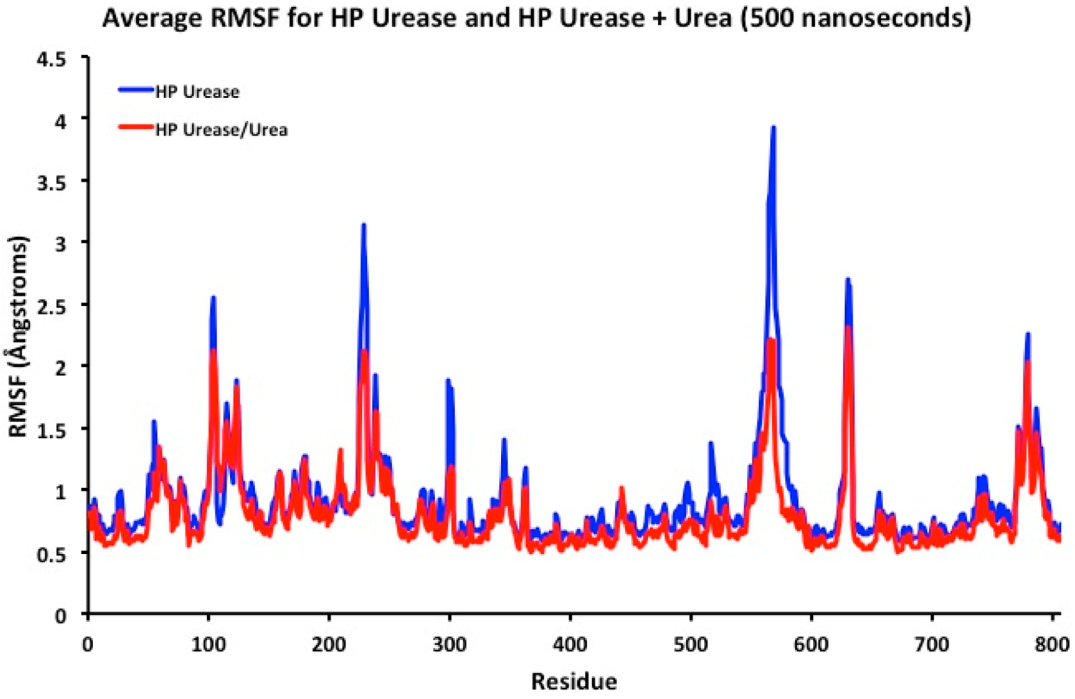

Figure 1. Overlay of the average rmsf plots for HP urease and HP urease in 10.5 M aqueous urea 500 ns simulations.

equilibration, the distribution is 57.0 and 43.0% between nonpolar and polar, respectively. The distribution remains relatively unchanged throughout the 500 ns simulation (56.7 and 43.3%, respectively, at the end of the simulation).

rmsf. Over the course of the simulation, we observe high-rmsf regions that differ slightly from those observed in the aqueous HPU simulation, and the average rmsf values for the urea run were decreased in comparison to those for the original aqueous HPU simulation (Figure 1). One check for the denaturation of the protein was observation of the average rmsf at 100 ns intervals (Figures S10–S14 of the Supporting Information). While there is a modest increase in rmsf from 100 to 200 ns, there is no increase in average rmsf for the remainder of the simulation. All of the high-rmsf regions are found on the surface of the protein and reside mostly on the β-chain, which envelops the protein. These high-rmsf regions form horseshoes around the protein and lead to the opening of the active site, of which the loop region is a high-rmsf region. These regions contain multiple polar residues and bonds, making them good binding candidates for the highly polar urea molecule.

We compared rmsf values of the HP run in a 10.5 M aqueous urea solution to those of our earlier HP urease run in water and observed that the baseline rmsf value is approximately the same for both. The high rmsf values are larger for the original run than for the run with urea. In the original aqueous run, the region that had the highest rmsf value was the loop region while the region with the highest rmsf value on the urea run was that of residues α387–395 (625–633), which is the "exhaust flap", whereas in the aqueous simulation, the loop of the active site-covering flap had the highest rmsf. The exhaust flap of the urease run has a rmsf slightly higher than that of both the loop of the active site-covering flap [residues α326–330 (564–568)] and that of the ancillary flap [residues α533–553 (771–791)]. In the original run, there is a region of high rmsf that resides on the interior of the protein, lining the hollow region, composed of residues α60–65 (298–303) that is not observed in the HP urease run in aqueous urea. For the most part, the urea run has lower rmsf values, indicating the protein moves but not as much as the original run and that it is not being denatured by the urea.[50]

These regions of high rmsf, particularly those of the β-chain, form a horseshoe-shaped region on the adjacent dimer that surrounds the loop of the active site-covering flap (Figure 2). In these regions, the rmsf of the urea run is larger than the average

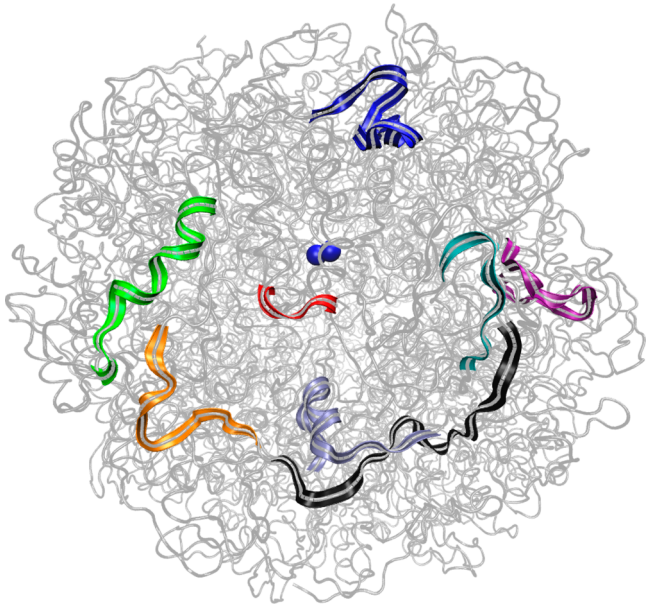

Figure 2. Horseshoe of high-rmsf regions surrounding the loop (residues 564–568) of the active site-covering flap (D4 and D5 refer to the dimer on which the residues are located): 564–568, red (D4); 771–791, blue (D4); 55–68, green (D5); 100–111, orange (D5); 113–130, black (D5); 177–184, cyan (D5); 222–238, purple (D5); 239–255, ice blue (D5).

DOI: 10.1021/acs.biochem.5b00078
Biochemistry 2015, 54, 4121–4130

Table 4. Protein Average rmsf's, Average rmsf's of Individual Horseshoe Regions, and Percentage Differences between Protein Average rmsf and Each Horseshoe Region

horseshoe region	residues	simulation type	average rmsf of protein	average rsmf of region	% change in rmsf
1	55−68	aqueous	0.916604409	1.1623076	126.805813
		10.5 M urea	0.798302337	1.0945442	137.108984
2	100−111	aqueous	0.916604409	1.3467284	146.925807
		10.5 M urea	0.798302337	1.4338710	179.615036
3	113−130	aqueous	0.916604409	1.2953326	141.318614
		10.5 M urea	0.798302337	1.2819089	160.579385
4	177−184	aqueous	0.916604409	1.1349468	123.820796
		10.5 M urea	0.798302337	1.0266528	128.604511
5	222−238	aqueous	0.916604409	1.7738969	193.529174
		10.5 M urea	0.798302337	1.4463798	181.181966
6	239−255	aqueous	0.916604409	1.1158668	121.739197
		10.5 M urea	0.798302337	1.0862892	136.074914
7	771−791	aqueous	0.916604409	1.4691696	160.283940
		10.5 M urea	0.798302337	1.3167437	164.942992

rmsf by a percentage greater than the corresponding increase observed in the aqueous simulation (Table 4). We find that the horseshoe region attracts molecules of urea (*vide infra*) and contains three points that are equidistant from the loop of the active site-covering flap. We hypothesize that this could allow for the shuttling of urea molecules toward the active site for subsequent entry and possibly facilitate transport of urea to the active site region. Urea is a highly proficient enzyme (k_{cat} = 1650 s^{-1}), which requires a high flux of substrate molecules reaching the active site.[51] These high-rmsf regions are on the surface, and we have done extensive studies of the number of urea molecules that interact with these areas throughout the entire simulation (*vide infra*). These horseshoes are symmetrically oriented about the dodecameric structure of *H. pylori* urease as shown in Figure S91 of the Supporting Information.

Visual observation of the MD simulation appeared to suggest the possibility of significant interactions between nonpolar residues on the surface of the enzyme and urea molecules. With regard to the high-RMSF horseshoe regions of the enzyme, it initially appears that there is little difference in interactive behavior of nonpolar residues and polar or charged residues with urea molecules in the local environment. However, observing the urea molecules discussed previously to have traveled along the horseshoe before descending into the active site cavity, one notes that these urea molecules interact most frequently with Pro, Met, and Leu, particularly if their descent into and subsequent activity within the active site is clear from visual observation. Whether these nonpolar residues play a particularly vital role in urea shuttling is not yet clear (the urea was also shown to interact with Lys and Ser with similar frequency), but investigation via alternate strategies should be considered. The nonpolar residues of this high-rmsf horseshoe region were then compared to those of a low-rmsf region, in this case, the nonpolar residues within the section of residues 400−500. A clear increase in the quantity of urea molecules interacting with nonpolar residues is present within the high-rmsf region when compared to those a low-rmsf region. However, this appears to be the case for all residues within each respective region; as such, this may simply be a result of varying rmsf's, as opposed to a result inherent to the properties of the respective nonpolar residues. Regardless, additional evaluation is warranted; as it would be cumbersome to visually evaluate the behavior of each nonpolar residue across the length of the MD simulation, a more computationally oriented approach may be required.

Active Site Flap Characterization. We previously used a number of characterization techniques to provide evidence of the existence of three well-defined states for the active site flap. These studies focused on the three residue pairs relevant to the characterization of the active site flap: Ileα328/Alaβ170 (Ile566/Ala170), Hisα322/Glyα47 (His560/Gly285), and Gluα330/Alaβ173 (Glu568/Ala173). We first plotted critical separations between these residue pairs to probe the opening of the active site flap, revealing several flaps through the simulation, specifically flap 4, that exhibit three unique separation states. Subsequent free energy maps revealed clear local minima that were assigned to the unique flap states in the case of Ileα328/Alaβ170 (Ile566/Ala170). The other two pairs, however, featured no distinct minima at large separations. We suspected that this occurred due to the fact that the corresponding residues are contained within α-helices that unravel as the flap shifts states. Further study of the changes in secondary structure associated with each residue of interest resulted in observations consistent with this possibility. An expanded discussion of the active site flap is found at the conclusion of the Supporting Information.

Urea Distribution. To examine the distribution of urea molecules on the surface of the protein, we created a 1 $Å^3$ grid around urease, and at each point, we summed the number of urea molecules present over the entire 500 ns simulation. Overall, urea molecules are found in high-density around regions of high rmsf. The second point is that urea is found at the large ovoid holes to the hollow but at lower density at the holes lined by the α-helices. Urea seems to be found around both hydrophilic and hydrophobic residues. Urea is not found in the hollow at the center of the protein and is not observed until we reach a 19 Å radius from the center of mass of the protein. Urea mostly interacts with loop regions on the protein as opposed to α-helices.

First Solvation Shell. The composition of the first solvation shell was determined for the aqueous HPU and HPU plus aqueous urea simulations at 100 ns intervals along the respective trajectories, in addition to the equilibrated structures. The bulk solvent in our urea simulation includes 25321 water molecules and 4788 urea molecules, a water:urea ratio of 5.29:1. We chose to select any water or urea molecules within 2 Å of the protein surface as residing within the first

DOI: 10.1021/acs.biochem.5b00078
Biochemistry 2015, 54, 4121−4130

solvation shell (Table 5). Following equilibration and at points taken every 100 ns along the trajectory, the water:urea ratio at the protein surface is significantly lower than the ratio present in the bulk solvent. The highest ratio of 4.55 water molecules per urea molecule was observed following equilibration, and the ratio settled at nearly 4:1 for the remainder of the simulation. The total number of molecules present in the first solvation shell for the aqueous urea simulation was considerably less than the total in the aqueous HPU run, an observation easily accounted for by the relative sizes of the urea and water molecules. While the total number of urea molecules increased postequilibration, the ratio of water to urea remained much lower than that in the bulk solvent because of a corresponding increase in the number of water molecules. This can be attributed to the "structure-making" property of urea, which possesses eight potential hydrogen bonding sites and can order multiple water molecules while remaining in contact with the protein.

Table 5. Composition of the First Solvation Shell (water or urea molecules within 2 Å of the protein surface) for the Aqueous HPU and HPU/Aqueous Urea Simulations

	HPU	HPU with urea			
entry	water	water	urea	total	water:urea
equilibrated	6022	4359	957	5316	4.55
100 ns	7906	5461	1351	6812	4.04
200 ns	8114	5630	1319	6949	4.27
300 ns	8242	5675	1398	7073	4.06
400 ns	8252	5754	1469	7223	3.92
500 ns	8327	5710	1453	7163	3.93

Urea in Active Site Cavities. We further analyzed the trajectory to determine whether urea molecules were approaching any of the 12 active sites. In 10 of the 12 dimers, urea molecules are observed within 10 Å of the active site. In the active site of dimer 4, we see multiple urea molecules entering beginning at 346 ns, with urea coming within 6.7 Å of the pentacoordinate Ni^{2+} (Figure 3). This accumulation of urea in the active site cavity is in stark contrast to the small amount observed in the closed and semiopen states (Figures S44 and S45 of the Supporting Information). In the closed state at 100 ns, no urea is observed in the active site cavity (Figure S44 of the Supporting Information), as expected. At 250 ns, the active site-covering flap has been in the semiopen state for nearly 150 ns, and still only two urea molecules have begun to migrate into the cavity (Figure S45 of the Supporting Information). Only after the wide-open flap state has been achieved does the rapid migration of urea into the cavity commence for dimer 4. The observation of the large amount of urea in this particular dimer is noteworthy, as this is one of the active site-covering flaps that opens the widest, and opens at an earlier point in the simulation than the other 11. We see the largest influx of urea molecules in dimer 4 and dimer 5, two flaps that reach the wide-open state.

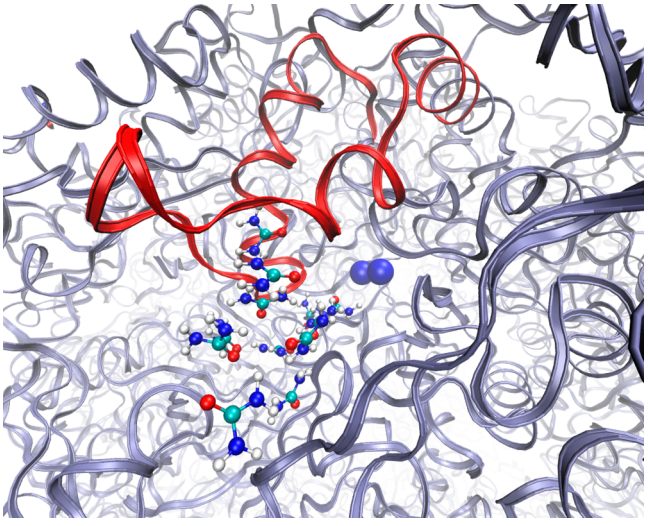

Figure 3. Snapshot showing accumulation of urea in the active site and flap of dimer 4 at 400 ns (wide-open flap state). Snapshots at 100 (closed) and 250 (semiopen) are included in the Supporting Information for comparison (Figures S44 and S45, respectively).

In dimers 4−8, we observe urea molecules within 7 Å of the pentacoordinate Ni^{2+}, some as close as 2.85 Å. In conjunction with the active site-covering flap of dimer 4 reaching the wide-open state at 346 ns, we further observe urea approaching the pentacoordinate Ni^{2+} at a distance of 6.7 Å (357 ns), a second molecule draws within 3.19 Å, and a third urea molecule is 3.85 Å from this nickel ion near the conclusion of the simulation. There was a large influx of urea within 10 Å of the fifth active site during the simulation, concomitant with the active site-covering flap reaching the wide-open state. For dimer 6, a urea molecule is within 10 Å of the pentacoordinate Ni^{2+} at 150 ns and draws within 3.4 Å of the pentacoordinate Ni^{2+} at 347 ns. This urea molecule remains within 10 Å of the metal ion for the remainder of the simulation. Furthermore, in dimer 3, urea is observed to approach within 9 Å of the pentacoordinate Ni^{2+}.

Residue separations indicate dimer 7 opens approximately 400 ns into the simulation [Ileα328/Alaβ170 (Ile566/Ala173) separation of 20−25 Å over the final 100 ns], corresponding to an observed influx of urea into the active site cavity over this duration. Flaps 1 and 10 stay closed throughout, and there is little urea observed to approach the active site. Flap 12 opens slightly over the final 100 ns [Ileα328/Alaβ170 (Ile566/Alaβ170) separation of 18 Å]; however, there was little influx of urea into the active site cavity.

In the active sites of dimers 5−7, while the quantity of urea observed is smaller than in dimer 4, urea molecules do approach the pentacoordinate Ni^{2+} much more closely, at distances of 3.19, 3.44, and 3.23 Å for active sites of dimers 5−7, respectively. Figure 4 depicts the approach of a urea molecule to the five-coordinate Ni^{2+} with the carbonyl in position for binding to the metal, a posited first step in the urea hydrolysis mechanism.[1,14,52]

Urea Residence Times and Saturation of High-rmsf Regions. For this analysis, we wrote a code that tracked the distance of every urea from every high-rmsf region selected and listed the urea molecules that are within 2 Å of these regions at nanosecond intervals. We chose 2 Å because it is a tight constraint, and this is necessary due to complications associated with attempting to detail all hydrogen bonding angles. Then we took the nine high-rmsf regions on the 12 dimers and binned the urea that resided for ≥10 ns. We constructed a histogram that shows the quantity of urea for different time intervals exceeding 10 ns over the entire simulation.

The region formed by residues β55−β68, which is one of the regions of the horseshoe closest to the loop of the active site-covering flap, does not display a large quantity of urea molecules that interact for an extended duration (Figure S46 of

DOI: 10.1021/acs.biochem.5b00078
Biochemistry 2015, 54, 4121−4130

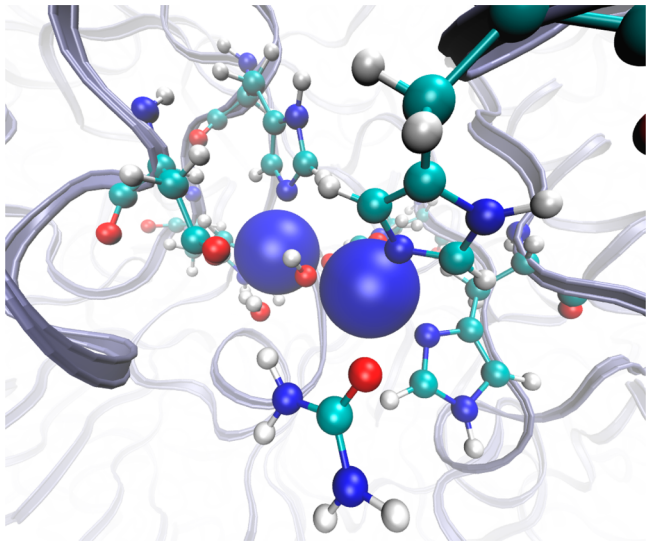

Figure 4. Urea molecule (bottom center of the image) nearing the pentacoordinate Ni^{2+} of dimer 5 at 331 ns.

the Supporting Information). Dimer 3 had 11 long residence urea molecules, and dimer 12 had only one such urea. Region β100−111 (100−111) is a loop connecting two β-regions that makes up part of the horseshoes. More than one molecule of urea per residue is in close contact with this region (Figure S47 of the Supporting Information). For the region composed of residues β113−130 (113−130), we see a much larger number of urea interactions (Figure S48 of the Supporting Information). In dimers 3 and 11, we have more than 100 urea molecules interacting for ≥10 ns. This region is the loop region located on the outside of the protein connecting regions of the β-chain found on the surface. Dimer 9 has no urea interacting for >10 ns. Region β177−184 (177−184) is one of the regions that are the closest three points of the horseshoe. All dimers except for dimer 11 have values between 1 and 32 long residence urea molecules, typically with only one such molecule (Figure S49 of the Supporting Information). Dimer 11 has 323 long residence urea molecules, which is the highest value observed. Region β222−238 (222−238) is a region found near the ovoid hole to the entrance of the hollow. There are three dimers with large numbers of urea molecules that interact, namely, dimers 3, 7, and 11 that come together to form one of the ovoid holes (Figure S50 of the Supporting Information). Region α1−17 (239−255) is the beginning of the α-chain and is the inner segment of the horseshoe and one of the three closest points to the active site-covering flap. This region is very near the active site flap of the adjacent dimer. In this particular histogram, we do not observe very high values of urea residing for >10 ns (Figure S51 of the Supporting Information). The dimer with the highest value is dimer 8, with 24 urea molecules that reside for >10 ns. Most of the dimers have 13 such urea molecules, with only two long residence urea molecules observed for dimer 1, which stays closed. These results are easily explained by the region's proximity to the loop of the active site flap.

We also compared the low-rmsf regions of the protein to the high-rmsf regions to ascertain whether there were as many interactions with urea throughout the simulation as were found in the high-rmsf regions. Most of the low-rmsf regions are not found on the surface of the protein and are therefore not as exposed to the solvating solution as are the high-rmsf regions that tend to reside on the enzyme exterior. The few regions that were exposed to the surface of the protein had very few urea molecules within a cutoff of 2 Å.

For example, within the region β30−38 (2466−2474) of dimer 4, only Leuβ38 (Leu2474) featured any noticeable interactions with urea molecules. Such interactions were few in number; interactions with only five unique urea molecules occurred throughout the entire simulation, which is low compared to the total number of urea molecules found in the bulk solvent, which contains around 4788 molecules. Given the high concentration of urea, it is inevitable for a few molecules to be within 2 Å of a residue on the protein's surface.

Region α326−330 (564−568) is the loop of the active site-covering flap and contains a very small amount of urea per residue (Figure S52 of the Supporting Information). The high-rmsf region formed by residues α387−395 (625−633) corresponds to the loop connecting two α-helices found in the back of the active site. This particular region does not seem to attract that many urea molecules throughout the simulation as borne out in Figure S53 of the Supporting Information. This is a logical occurrence due to the fact that the loop region is found on the inner segment of the protein. Furthermore, the loop is not near the active site flap and thereby cannot significantly contribute to shuttling urea into the active site; rather, it could facilitate exit shuttling of hydrolysis products. In the region composed of residues α533−553 (771−791), we observe that there is more than one urea molecule per residue for most of the dimers, except for dimers 4−6 (Figure S54 of the Supporting Information). Dimer 11 attracts 167 long residence urea molecules. There seems to be no correlation between the rmsf value and the number of urea molecules that interact. It does make sense for the active site loop not to have urea interact for an extended period of time, as this could attenuate active site entry rather than enhance it. The longest residence time urea molecules on the loop of the active site-covering flap are observed on flaps that remain closed throughout the simulation.

We observed the number of urea molecules that came within 2 Å of the high-rmsf regions, including the active site loop and the surrounding horseshoe region, as a function of time. Particular focus was applied to the differences in the number of urea molecules around the wide-open flap of dimer 5 and the closed flap of dimer 6. The loop region of the active site flap of dimer 5 attracts more urea molecules as the flap opens further. The same region for dimer 6, which remains closed for the duration of the simulation, has comparatively fewer urea molecules. Urea molecules approaching the high-rmsf regions comprising the horseshoe surrounding the loop of the active site-covering flap, which is located on adjacent dimers, were charted, as well. For the wide-open flap, there are more adsorbed urea molecules on average than in the horseshoe region surrounding the closed flap state. There are more urea molecules at the termini of the horseshoe surrounding the wide-open flap than at that of the closed flap, but the inner regions of the horseshoe have comparably similar urea activity in both dimers, with an only slight excess in the regions surrounding a wide-open flap.

High-rmsf Regions and Active Site Entry. Having recognized the entry of urea into the active site and identifying specific urea molecules that draw near to the pentacoordinate Ni^{2+}, we monitored the position of these molecules before their entry into the active site. One common feature of the pathway undertaken by these urea molecules that accessed the active site

DOI: 10.1021/acs.biochem.5b00078
Biochemistry 2015, 54, 4121−4130

is periods of interaction with multiple high-rmsf regions on the exterior of the protein. We hypothesize that the outer residues of the protein function in a dual-fold manner, first to attract urea molecules and then to shuttle the substrate molecules toward the active site-covering flap. We will detail the travels of two urea molecules as examples supporting our hypothesis; however, these are not the only occurrences of this phenomenon. In total, there are nine urea molecules that migrate within 3 Å of the bridging hydroxide, a distance that we selected as the threshold for having completely accessed the active site cavity and becoming a likely hydrolysis candidate. All urea molecules that migrated within 3 Å (nine) of the bridging hydroxide entered the active site following interaction with the high-rmsf horseshoe region, subsequently approaching the loop of the active site-covering flap and finally descending into the active site. Additionally, nine other molecules approach the 3 Å threshold and follow the same entry pathway but do not approach as close to the active site as the first nine urea molecules.

Urea 20177 spends a significant portion of the simulation traversing the high-rmsf regions. Following periods of interaction with other high-rmsf regions, this molecule begins to interact with β-chain residues 222−238 of chain 1 at 318 ns before shuttling to residues 564−568 (α326−330) of α-chain 1 at 322−324 ns. Subsequently, the urea molecule enters the active site where it remains for the duration of the simulation in the proximity of the pentacoordinate Ni^{2+} ion. Snapshots of this sequence are shown in Figure 5. Of particular note in this sequence is that while the urea escapes from the loop of the active site-covering flap upon its initial contact, the horseshoe recaptures the molecule and shuttles it back for active site entry. Our second molecule, urea 13099, is observed to behave like the previously described urea, although with more observed escape and recapture events between the loop of the active site-covering flap and the high-rmsf regions of the horseshoe over the final 104 ns of the simulation. First, it is drawn to the inside portion of the horseshoe at 396 ns, after which occur a series of transfer events in which the urea molecule bounces between the interior portion of the horseshoe and the loop of the active site-covering flap through 406 ns. Subsequently, the urea molecule is shuttled to other high-rmsf regions comprising the horseshoe. The final urea transfer to the loop of the active site-covering flap occurs at 446 ns, and following this transfer, the molecule descends into the active site cavity for the remainder of the simulation. These travels are displayed in Figures S92−S97 of the Supporting Information.

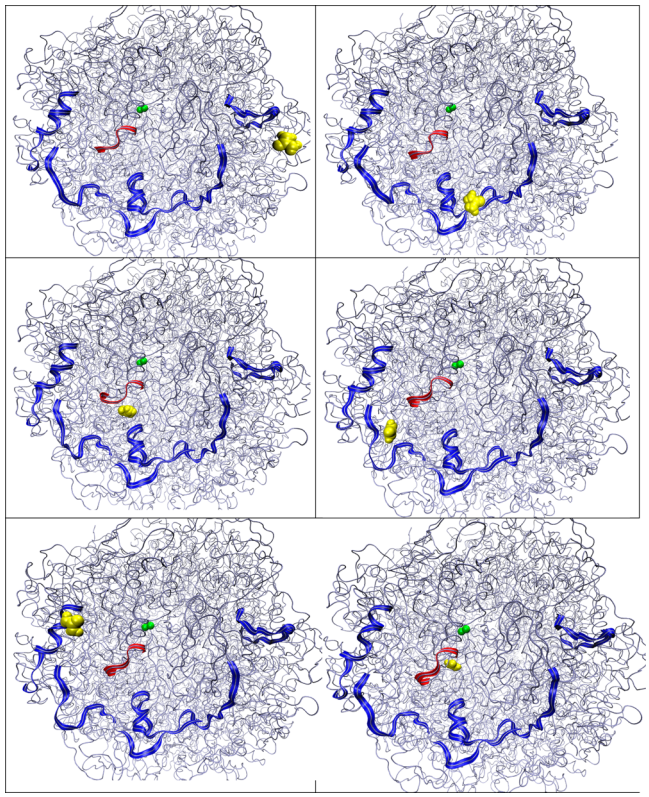

Figure 5. Snapshots of urea molecule 20177 interacting with regions of high rmsf from 318 to 328 ns before descending into the active site cavity. High-rmsf regions comprising the horseshoe are shown as blue ribbons. The loop of the active site-covering flap is depicted as a red ribbon. The Ni^{2+} ions are depicted as green van der Waals spheres, and the urea molecule is depicted as a collection of yellow van der Waals spheres. The snapshots correspond to 318 ns (top left), 319 ns (top right), 321 ns (middle left), 322 ns (middle right), 324 ns (bottom left), and 328 ns (bottom right).

CONCLUSIONS

Herein, we have presented the results and analysis of a molecular dynamics simulation of HP urease in a 10.5 M aqueous urea solution over 500 ns. We compared the results to an extension of our previous study, a 400 ns MD simulation[30] of aqueous HP urease that we lengthened by 100 ns. The flap motion that was previously observed, including the identification of a wide-open flap state, was also observed in the active site-covering flaps over the course of our aqueous urea simulation. A direct correlation between the flaps opening and the entry of urea is observed, where a wider opening of the flap results in the entry of significantly more urea into the active site cavity. It appears that urea cannot access the active site using the semiopen state observed experimentally,[7] suggesting that the wide-open state observed computationally is necessary for active site ingress by urea. We comment on our observations regarding the regions of high rmsf, which form horseshoes about the loops of the active site-covering flaps. We also analyzed the first solvation shell to ensure the protein is not denaturing. In the bulk solvent, the water:urea ratio is 5.29:1; however, the first solvation shell (2 Å from the protein surface) generally has a ratio of 4:1 over the duration of the run.

The most unique and intriguing observation over the course of this research is the horseshoe surrounding the active site-covering loops that is created by the high-rmsf regions of the β-chain and the mechanism via which urea is shuttled into the active site. There are three points specifically on the horseshoe that are closest to the active site flap that seemingly guide urea to the loop of the active site flap and allow subsequent entry into the active site cavity. From this new observation, we can now target other regions of the protein that may negatively affect the enzymatic hydrolysis of urea. It is feasible that binding or otherwise reducing the urea attracting capability of these three closest points could attenuate the entry of urea into the active site. Further disruption or severing of the residues comprising the horseshoe, either enzymatically or via other means, could affect the urea hydrolysis process, as well. This could be further evaluated by creating a mutated version of *H. pylori* urease by altering one or more of the high-rmsf residues comprising the horseshoe regions.

DOI: 10.1021/acs.biochem.5b00078
Biochemistry 2015, 54, 4121−4130

■ ASSOCIATED CONTENT

Supporting Information

Additional plots containing information about rmsd's, rmsf's, residue separations, free energy maps, radii of gyration, and sodium ion distribution. The Supporting Information is available free of charge on the ACS Publications website at DOI: 10.1021/acs.biochem.5b00078.

■ AUTHOR INFORMATION

Corresponding Author

*E-mail: kmerz1@gmail.com.

Funding

We acknowledge the financial support from the U.S. National Institutes of Health (RO1 GM066859). M.S.M. thanks the National Science Foundation for support in the form of a graduate research fellowship.

Notes

The authors declare no competing financial interest.

■ ACKNOWLEDGMENTS

M.S.M. gratefully acknowledges support from the University of Florida Disability Resource Center and Sean Jones. We thank the University of Florida HPC center for generous allocations of GPU time. We thank Dr. Dhruva Chakravorty and Dr. Billy Miller for many useful discussions during this project.

■ REFERENCES

(1) Karplus, P. A., Pearson, M. A., and Hausinger, R. P. (1997) 70 years of crystalline urease: What have we learned? *Acc. Chem. Res. 30*, 330−337.

(2) Mobley, H. L. T., Island, M. D., and Hausinger, R. P. (1995) Molecular-Biology of Microbial Ureases. *Microbiol. Rev. 59*, 451−480.

(3) Pinkse, M. W. H., Maier, C. S., Kim, J. I., Oh, B. H., and Heck, A. J. R. (2003) Macromolecular assembly of *Helicobacter pylori* urease investigated by mass spectrometry. *J. Mass Spectrom. 38*, 315−320.

(4) Buck, G. E. (1990) *Campylobacter pylori* and Gastroduodenal Disease. *Clin. Microbiol. Rev. 3*, 1−12.

(5) Covacci, A., Telford, J. L., Del Giudice, G., Parsonnet, J., and Rappuoli, R. (1999) *Helicobacter pylori* virulence and genetic geography. *Science 284*, 1328−1333.

(6) Dunn, B. E., Cohen, H., and Blaser, M. J. (1997) *Helicobacter pylori*. *Clin. Microbiol. Rev. 10*, 720−741.

(7) Ha, N. C., Oh, S. T., Sung, J. Y., Cha, K. A., Lee, M. H., and Oh, B. H. (2001) Supramolecular assembly and acid resistance of *Helicobacter pylori* urease. *Nat. Struct. Biol. 8*, 505−509.

(8) Chey, W. D., and Wong, B. C. Y. (2007) American college of gastroenterology guideline on the management of *Helicobacter pylori* infection. *Am. J. Gastroenterol. 102*, 1808−1825.

(9) Malfertheiner, P., Bazzoli, F., Delchier, J. C., Celinski, K., Giguere, M., Riviere, M., Megraud, F., and Grp, P. S. (2011) *Helicobacter pylori* eradication with a capsule containing bismuth subcitrate potassium, metronidazole, and tetracycline given with omeprazole versus clarithromycin-based triple therapy: A randomised, open-label, non-inferiority, phase 3 trial. *Lancet 377*, 905−913.

(10) Estiu, G., and Merz, K. M. (2004) Enzymatic catalysis of urea decomposition: Elimination or hydrolysis? *J. Am. Chem. Soc. 126*, 11832−11842.

(11) Estiu, G., and Merz, K. M. (2006) Catalyzed decomposition of urea. Molecular dynamics simulations of the binding of urea to urease. *Biochemistry 45*, 4429−4443.

(12) Estiu, G., Suarez, D., and Merz, K. M. (2006) Quantum mechanical and molecular dynamics simulations of ureases and Zn β-lactamases. *J. Comput. Chem. 27*, 1240−1262.

(13) Estiu, G. L., Suarez, D., Diaz, N., and Merz, K. M. (2004) Molecular dynamics simulations of urea-inhibited urease. *Abstracts of Papers of the American Chemical Society 228*, U295.

(14) Estiu, L. G., and Merz, K. M. (2004) Molecular dynamics simulations of urease catalysis. *Abstracts of Papers of the American Chemical Society 227*, U1006.

(15) Abid, O. U. R., Babar, T. M., Ali, F. I., Ahmed, S., Wadood, A., Rama, N. H., Uddin, R., Zaheer-ul-Haq, Khan, A., and Choudhary, M. I. (2010) Identification of Novel Urease Inhibitors by High-Throughput Virtual and in Vitro Screening. *ACS Med. Chem. Lett. 1*, 145−149.

(16) Valdez, C. E., and Alexandrova, A. N. (2012) Why Urease Is a Di-Nickel Enzyme whereas the CcrA β-Lactamase Is a Di-Zinc Enzyme. *J. Phys. Chem. B 116*, 10649−10656.

(17) Font, M., Dominguez, M. J., Sanmartin, C., Palop, J. A., San-Francisco, S., Urrutia, O., Houdusse, F., and Garcia-Mina, J. M. (2008) Structural characteristics of phosphoramide derivatives as urease inhibitors. Requirements for activity. *J. Agric. Food Chem. 56*, 8451−8460.

(18) Dominguez, M. J., Sanmartin, C., Font, M., Palop, J. A., Francisco, S. S., Urrutia, O., Houdusse, F., and Garcia-Mina, J. M. (2008) Design, synthesis, and biological evaluation of phosphoramide derivatives as urease inhibitors. *J. Agric. Food Chem. 56*, 3721−3731.

(19) Xiao, Z. P., Wang, X. D., Peng, Z. Y., Huang, S., Yang, P., Li, Q. S., Zhou, L. H., Hu, X. J., Wu, L. J., Zhou, Y., and Zhu, H. L. (2012) Molecular Docking, Kinetics Study, and Structure-Activity Relationship Analysis of Quercetin and Its Analogous as *Helicobacter pylori* Urease Inhibitors. *J. Agric. Food Chem. 60*, 10572−10577.

(20) Pace, N. C., and Tanford, C. (1968) Thermodynamics of Unfolding of β-Lactoglobulin A in Aqueous Urea Solutions between 5 and 55°. *Biochemistry 7*, 198−208.

(21) Creighton, T. E. (1977) Effects of Urea and Guanidine.Hcl on Folding and Unfolding of Pancreatic Trypsin-Inhibitor. *J. Mol. Biol. 113*, 313−328.

(22) Muthuselvi, L., Miller, R., and Dhathathreyan, A. (2008) How does urea really denature myoglobin? *Chem. Phys. Lett. 465*, 126−130.

(23) TiradoRives, J., Orozco, M., and Jorgensen, W. L. (1997) Molecular dynamics simulations of the unfolding of barnase in water and 8 M aqueous urea. *Biochemistry 36*, 7313−7329.

(24) Caflisch, A., and Karplus, M. (1999) Structural details of urea binding to barnase: A molecular dynamics analysis. *Structure 7*, 477−488.

(25) Camilloni, C., Rocco, A. G., Eberini, I., Gianazza, E., Broglia, R. A., and Tiana, G. (2008) Urea and guanidinium chloride denature protein L in different ways in molecular dynamics simulations. *Biophys. J. 94*, 4654−4661.

(26) Cai, Z., Li, J., Yin, C., Yang, Z., Wu, J., and Zhou, R. (2014) Effect of Urea Concentration on Aggregation of Amyloidogenic Hexapeptides (NFGAIL). *J. Phys. Chem. B 118*, 48−57.

(27) Moeser, B., and Horinek, D. (2014) Unified Description of Urea Denaturation: Backbone and Side Chains Contribute Equally in the Transfer Model. *J. Phys. Chem. B 118*, 107−114.

(28) Stumpe, M. C., and Grubmuller, H. (2007) Aqueous urea solutions: Structure, energetics, and urea aggregation. *J. Phys. Chem. B 111*, 6220−6228.

(29) Bandyopadhyay, D., Mohan, S., Ghosh, S. K., and Choudhury, N. (2014) Molecular Dynamics Simulation of Aqueous Urea Solution: Is Urea a Structure Breaker? *J. Phys. Chem. B 118*, 11757−11768.

(30) Minkara, M. S., Ucisik, M. N., Weaver, M. N., and Merz, K. M. (2014) Molecular Dynamics Study of *Helicobacter pylori* Urease. *J. Chem. Theory Comput. 10*, 1852−1862.

(31) Roberts, B. P., Miller, B. E., Roitberg, A. E., and Merz, K. M. (2012) Wide-Open Flaps are Key to Urease Activity. *J. Am. Chem. Soc. 134*, 9934−9937.

(32) *The PyMOL Molecular Graphics System*, version 1.3r1 (2010) Schrodinger, LLC., Portland, OR.

(33) H++ Protonation Server, h. b. c. v. e. H. H++ Protonation Server.

DOI: 10.1021/acs.biochem.5b00078
Biochemistry 2015, 54, 4121−4130

(34) Anandakrishnan, R., Aguilar, B., and Onufriev, A. V. (2012) H+ +3.0: Automating pK prediction and the preparation of biomolecular structures for atomistic molecular modeling and simulations. *Nucleic Acids Res. 40*, W537−W541.
(35) Myers, J., Grothaus, G., Narayanan, S., and Onufriev, A. (2006) A simple clustering algorithm can be accurate enough for use in calculations of pKs in macromolecules. *Proteins 63*, 928−938.
(36) Gordon, J. C., Myers, J. B., Folta, T., Shoja, V., Heath, L. S., and Onufriev, A. (2005) H++: A server for estimating pK_as and adding missing hydrogens to macromolecules. *Nucleic Acids Res. 33*, W368−W371.
(37) Case, D. A., Darden, T. A., Cheatham, T. E. I., Simmerling, C. L., Wang, J., Duke, R. E., Luo, R., Walker, R. C., Zhang, W., Merz, K. M., Roberts, B., Wang, B., Hayik, S., Roitberg, A., Seabra, G., Kolossvai, I., Wong, K. F., Paisani, F., Vanicek, J., Liu, J., Wu, X., Brozell, S. R., Steinbrecher, T., Gohlke, H., Cai, Q., Ye, X., Wang, J., Hseih, M.-J., Cui, G., Roe, D. R., Mathews, D. H., Seetin, M. G., Sagui, C., Babin, V., Luchko, T., Gusarov, S., Kovalenko, A., and Kollman, P. A. (2010) *AMBER 11*, University of California, San Francisco.
(38) Price, D. J., and Brooks, C. L. (2004) A modified TIP3P water potential for simulation with Ewald summation. *J. Chem. Phys. 121*, 10096−10103.
(39) Roberts, B. P., Miller, B. R., Roitberg, A. E., and Merz, K. M. (2012) Wide-Open Flaps Are Key to Urease Activity. *J. Am. Chem. Soc. 134*, 9934−9937.
(40) Merz, K. M. (1991) CO_2 Binding to Human Carbonic Anhydrase-II. *J. Am. Chem. Soc. 113*, 406−411.
(41) Hornak, V., Abel, R., Okur, A., Strockbine, B., Roitberg, A., and Simmerling, C. (2006) Comparison of multiple amber force fields and development of improved protein backbone parameters. *Proteins 65*, 712−725.
(42) Lindorff-Larsen, K., Piana, S., Palmo, K., Maragakis, P., Klepeis, J. L., Dror, R. O., and Shaw, D. E. (2010) Improved side-chain torsion potentials for the Amber ff99SB protein force field. *Proteins 78*, 1950−1958.
(43) Ryckaert, J. P., Ciccotti, G., and Berendsen, H. J. C. (1977) Numerical-Integration of Cartesian Equations of Motion of a System with Constraints: Molecular-Dynamics of N-Alkanes. *J. Comput. Phys. 23*, 327−341.
(44) Case, D. A., Darden, T. A., Cheatham, T. E. I., Simmerling, C. L., Wang, J., Duke, R. E., Luo, R., Walker, R. C., Zhang, W., Merz, K. M., Roberts, B., Hayik, S., Roitberg, A., Seabra, G., Swails, J., Goetz, A. W., Kolossvai, I., Wong, K. F., Paisani, F., Vanicek, J., Wolf, R. M., Liu, J., Wu, X., Brozell, S. R., Steinbrecher, T., Gohlke, H., Cai, Q., Ye, X., Wang, J., Hseih, M.-J., Cui, G., Roe, D. R., Mathews, D. H., Seetin, M. G., Salomon-Ferrer, R., Sagui, C., Babin, V., Luchko, T., Gusarov, S., Kovalenko, A., and Kollman, P. A. (2012) *AMBER 12*, University of California, San Francisco.
(45) Goetz, A. W., Williamson, M. J., Xu, D., Poole, D., Le Grand, S., and Walker, R. C. (2012) Routine Microsecond Molecular Dynamics Simulations with AMBER on GPUs. 1. Generalized Born. *J. Chem. Theory Comput. 8*, 1542−1555.
(46) Hubbard, S., and Thornton, J. (2014) *Naccess*.
(47) Lee, B., and Richards, F. M. (1971) Interpretation of Protein Structures: Estimation of Static Accessibility. *J. Mol. Biol. 55*, 379−400.
(48) Joosten, R. P., te Beek, T. A., Krieger, E., Hekkelman, M. L., Hooft, R. W., Schneider, R., Sander, C., and Vriend, G. (2011) A series of PDB related databases for everyday needs. *Nucleic Acids Res. 39*, D411−D419.
(49) Kabsch, W., and Sander, C. (1983) Dictionary of Protein Secondary Structure: Pattern-Recognition of Hydrogen-Bonded and Geometrical Features. *Biopolymers 22*, 2577−2637.
(50) Candotti, M., Perez, A., Ferrer-Costa, C., Rueda, M., Meyer, T., Gelpi, J. L., and Orozco, M. (2013) Exploring Early Stages of the Chemical Unfolding of Proteins at the Proteome Scale. *PLoS Comput. Biol. 9*, e1003393.
(51) Wolfenden, R., and Snider, M. J. (2001) The depth of chemical time and the power of enzymes as catalysts. *Acc. Chem. Res. 34*, 938−945.
(52) Carlsson, H., and Nordlander, E. (2010) Computational Modeling of the Mechanism of Urease. *Bioinorg. Chem. Appl.*, 364891.

DOI: 10.1021/acs.biochem.5b00078
Biochemistry 2015, 54, 4121−4130